Structural Basis for Aβ₁₋₄₂ Toxicity Inhibition by Aβ C-Terminal Fragments: Discrete Molecular Dynamics Study

B. Urbanc[1]*, M. Betnel[2], L. Cruz[1], H. Li[3], E. A. Fradinger[3], B. H. Monien[3] and G. Bitan[3,4]

[1]*Department of Physics, Drexel University, Philadelphia, PA 19104, USA*
[2]*Department of Physics, Boston University, Boston, MA 02215, USA*
[3]*Department of Neurology, David Geffen School of Medicine, University of California, Los Angeles, CA 90095-7334, USA*
[4]*Molecular Biology Institute and Brain Research Institute, University of California, Los Angeles, CA 90095-7334, USA*

Amyloid β-protein (Aβ) is central to the pathology of Alzheimer's disease. Of the two predominant Aβ alloforms, Aβ₁₋₄₀ and Aβ₁₋₄₂, the latter forms more toxic oligomers. C-terminal fragments (CTFs) of Aβ were recently shown to inhibit Aβ₁₋₄₂ toxicity *in vitro*. Here, we studied Aβ₁₋₄₂ assembly in the presence of three effective CTF inhibitors and an ineffective fragment, Aβ₂₁₋₃₀. Using a discrete molecular dynamics approach that recently was shown to capture key differences between Aβ₁₋₄₀ and Aβ₁₋₄₂ oligomerization, we compared Aβ₁₋₄₂ oligomer formation in the absence and presence of CTFs or Aβ₂₁₋₃₀ and identified structural elements of Aβ₁₋₄₂ that correlated with Aβ₁₋₄₂ toxicity. CTFs co-assembled with Aβ₁₋₄₂ into large heterooligomers containing multiple Aβ₁₋₄₂ and inhibitor fragments. In contrast, Aβ₂₁₋₃₀ co-assembled with Aβ₁₋₄₂ into heterooligomers containing mostly a single Aβ₁₋₄₂ and multiple Aβ₂₁₋₃₀ fragments. The CTFs, but not Aβ₂₁₋₃₀, decreased the β-strand propensity of Aβ₁₋₄₂ in a concentration-dependent manner. CTFs and Aβ₂₁₋₃₀ had a high binding propensity to the hydrophobic regions of Aβ₁₋₄₂, but only CTFs were found to bind the Aβ₁₋₄₂ region A2–F4. Consequently, only CTFs but not Aβ₂₁₋₃₀ reduced the solvent accessibility of Aβ₁₋₄₂ in region D1–R5. The reduced solvent accessibility of Aβ₁₋₄₂ in the presence of CTFs was comparable to the solvent accessibility of Aβ₁₋₄₀ oligomers formed in the absence of Aβ fragments. These findings suggest that region D1–R5, which was more exposed to the solvent in Aβ₁₋₄₂ than in Aβ₁₋₄₀ oligomers, is involved in mediating Aβ₁₋₄₂ oligomer neurotoxicity.

© 2011 Elsevier Ltd. All rights reserved.

Corresponding author. E-mail address: brigita@drexel.edu.
Present addresses: E. A. Fradinger, Department of Biology, Whittier College, 13406 East Philadelphia Street, Whittier, CA 90608, USA; B. H. Monien, Deutsches Institut für Ernährungsforschung Potsdam-Rehbrücke, Abteilung Ernährungstoxikologie, Arthur-Scheunert-Allee 114-116, 14558 Nuthetal, Germany.
Abbreviations used: AD, Alzheimer's disease; Aβ, amyloid β-protein; DMD, discrete molecular dynamics; CTF, C-terminal fragment; DLS, dynamic light scattering; SASA, solvent-accessible surface area.

Introduction

Alzheimer's disease (AD) is an irreversible, progressive neurodegenerative disorder that is the dominant cause of dementia in the elderly. One of the hallmarks of AD is accumulation of extracellular senile plaques, which contain fibrillar aggregates of amyloid β-protein (Aβ). Genetic, pathologic, and biochemical evidence strongly supports the hypothesis that low-order oligomeric assemblies of Aβ, rather than fibrils, are the proximate neurotoxic

agents in AD.[1–7] The majority of Aβ oligomers were found to be neurotoxic,[8] and certain oligomers decreased neuronal viability 10- to 100-fold more strongly than Aβ fibrils.[9] Aβ$_{1-40}$ and Aβ$_{1-42}$, the major Aβ alloforms in the brain, differ by the presence of two amino acids, I41 and A42, at the C-terminus of the latter. Aβ$_{1-42}$ aggregates faster,[10,11] forms more toxic assemblies,[5] and is genetically linked to aggressive, early-onset familial forms of AD.[12] Cross-linking studies showed that Aβ$_{1-42}$ forms pentamers and hexamers (paranuclei) and multiples of paranuclei, including dodecamers and octadecamers, whereas Aβ$_{1-40}$ exists as a mixture of monomers through tetramers.[13] These observations have been confirmed independently by ion-mobility spectrometry/mass spectrometry.[14,15] Interestingly, Aβ dodecamers, which putatively form by self-association of two paranuclei, have been detected *in vivo* in several independent studies.[16–19]

In recent years, an *ab initio* discrete molecular dynamics (DMD) approach[20] using a four-bead protein model and residue-specific hydropathic interactions offered important insights into the folding and assembly of Aβ$_{1-40}$ and Aβ$_{1-42}$.[21–25] This approach recapitulated the essential, experimentally observed differences between the folding and oligomerization of Aβ$_{1-40}$ and Aβ$_{1-42}$ and demonstrated that Aβ$_{1-42}$ but not Aβ$_{1-40}$ oligomerization was driven primarily through intermolecular interactions involving the C-terminal region (I31–A42).[22,23,25] The DMD approach also predicted a quasi-stable turn at the C-terminus of Aβ$_{1-42}$, which does not occur in Aβ$_{1-40}$,[22] a prediction that was supported by several experimental studies.[26–30] In a most recent study, Streltsov *et al.* reported the first X-ray structure of the Aβ$_{18-41}$ tetramer encapsulated in a shark Ig new antigen receptor, which resembles the DMD-derived oligomeric structures.[31]

The DMD findings have led to a hypothesis that C-terminal fragments (CTFs) of Aβ$_{1-42}$ may interfere with Aβ$_{1-42}$ oligomerization. Recently, we reported that Aβ$_{1-42}$ CTFs ranging from Aβ$_{29-42}$ to Aβ$_{39-42}$, as well as Aβ$_{30-40}$, attenuated Aβ$_{1-42}$ neurotoxicity in neuronal cell culture.[32,33] We also investigated the aqueous solubility, aggregation kinetics, and morphology of CTFs[33] and found that their aggregation propensity correlated with the previously reported[34] tendency to form β-hairpin structures, whereas their ability to inhibit Aβ$_{1-42}$-induced neurotoxicity correlated with a tendency to form an irregular "coil–turn" structure.[33] Dynamic light-scattering (DLS) data revealed that two Aβ$_{1-42}$ oligomer populations, which were scarcely populated in the absence of inhibitors, were enhanced by CTFs in an inhibitor-specific manner. In particular, stabilization of the smaller of the two Aβ$_{1-42}$/CTF heterotypic assembly populations with a hydrodynamic radius of 8–12 nm correlated with the degree of toxicity inhibition.[35] Stabilization of nontoxic

Aβ$_{1-42}$ assemblies might thus be a promising strategy for designing Aβ$_{1-42}$ toxicity inhibitors.[35] A similar mechanism was found for several other inhibitors, including scyllo-inositol[36–38] benzothiazole derivatives,[39] and the polyphenols epigallocatechin-3-gallate,[40,41] resveratrol,[42] myricetin, and nordihydroguaiaretic acid.[39] However, the mode of interaction of inhibitors with Aβ$_{1-42}$ and the structural changes in Aβ$_{1-42}$ that are required for a successful toxicity inhibition are unknown.

Our preliminary DMD study of Aβ$_{1-42}$ assembly in the presence of Aβ$_{29-42}$, Aβ$_{31-42}$, or Aβ$_{39-42}$, using Aβ$_{1-42}$/CTF molar concentration ratios of up to 1:2, demonstrated that these CTFs inserted themselves among Aβ$_{1-42}$ peptides, reducing their intermolecular contacts.[32] Inhibition of Aβ$_{1-42}$ toxicity by CTFs in a cell culture was concentration dependent and most efficient at the Aβ$_{1-42}$/CTF molar concentration ratio of ~1:10. Here, we applied the DMD approach to examine the assembly of Aβ$_{1-42}$ in the presence of three CTFs that efficiently inhibited Aβ$_{1-42}$ toxicity and a control peptide, Aβ$_{21-30}$, which had no effect on Aβ$_{1-42}$ toxicity,[33] at several Aβ$_{1-42}$/Aβ$_{21-30}$ concentration ratios, including 1:10. We explored the effects of Aβ$_{31-42}$, Aβ$_{39-42}$, and two additional Aβ fragments (Aβ$_{30-40}$ and Aβ$_{21-30}$) that were not included into our prior DMD study[32] using an improved, recently reported parametrization of the DMD approach.[24,25] The aim of the present work was to explore structural elements involved in Aβ$_{1-42}$ toxicity inhibition by CTFs. To achieve that, we analyzed the Aβ$_{1-42}$ structures formed in the presence of effective inhibitors and compared them to Aβ$_{1-42}$ oligomers formed in the absence of inhibitors and in the presence of ineffective Aβ$_{21-30}$ fragments. We also compared the Aβ$_{1-42}$ assembly structures formed in the presence of Aβ fragments to Aβ$_{1-40}$ oligomer populations (formed in the absence of Aβ fragments). Based on the present computational results and previously reported toxicity data,[32,33] we propose a mechanism in which CTFs inhibit Aβ$_{1-42}$ toxicity by binding to specific regions of Aβ$_{1-42}$, reducing its ability to form a β structure, and interrupting putative interactions of Aβ$_{1-42}$ with its cellular targets.

Results

We selected four Aβ$_{X–Y}$ fragments to study their effect on Aβ$_{1-42}$ assembly. Of all the experimentally examined CTFs,[33] Aβ$_{31-42}$ was chosen because it was the strongest inhibitor of neurotoxicity.[32,33] Aβ$_{39-42}$, the shortest of all the CTFs under study, showed surprisingly high inhibition of neurotoxicity.[32] Aβ$_{30-40}$ was selected because its degree of Aβ$_{1-42}$ toxicity inhibition was comparable to that of the other two CTFs,[33] and Aβ$_{21-30}$, which did not inhibit

Aβ$_{1-42}$ toxicity in cell culture, was chosen as a control peptide.

We simulated Aβ$_{1-42}$ assembly in the presence of CTFs or Aβ$_{21-30}$ using a four-bead protein model with backbone hydrogen bonding and amino-acid-specific interactions, as described in Methods (see Supplementary Methods in Supplementary Material). We used the implicit solvent parameters $E_{HP}=0.3$ and $E_{CH}=0$ and physiological temperature estimate $T=0.13$, which recently has been shown to match well the *in vitro* temperature dependence of the average β-strand in Aβ$_{1-40}$ and Aβ$_{1-42}$ monomers[24] and the distinct oligomer size distributions of Aβ$_{1-40}$, Aβ$_{1-42}$, and their Arctic mutants, [E22G]Aβ$_{1-40}$ and [E22G]Aβ$_{1-40}$.[25] The total number of Aβ$_{1-42}$ and fragment peptides and simulation box sizes (Table I in Supplementary Material) were chosen to correspond to a total molar concentration of ~3–4 mM as used in the previous DMD studies.[22,25] Typical molar concentrations in *in vitro* studies are 10- to 100-fold lower than the total molar concentration in our computational study. Due to limitations in the total number of atoms and timescales that can currently be efficiently studied by computer simulations,[43] millimolar concentrations are required for proteins to interact with each other and thus form assemblies and to obtain sufficient statistics on the assembled structures. The effect of Aβ fragments on Aβ$_{1-42}$ assembly and the resulting structures were quantified and compared to unaltered Aβ$_{1-42}$ oligomer structures using data from the recently published work.[25]

In the description of our results below, the following abbreviations for specific Aβ regions are used: CHC, central hydrophobic cluster (L17–A21); MHR, mid-hydrophobic cluster (I31–M35); and CTR, C-terminal region (V39–A42).

Aβ$_{X-Y}$ and Aβ$_{1-42}$ associate into Aβ$_{1-42}$/Aβ$_{X-Y}$ heterooligomers

Initially separated monomeric Aβ$_{1-42}$ and toxicity inhibitor Aβ$_{30-40}$, Aβ$_{31-42}$, or Aβ$_{39-42}$ (Fig. 1a) associated first into small Aβ$_{1-42}$/CTF heterooligomers of various sizes and compositions (Fig. 1b) and then into larger heterotypic assemblies (Fig. 1c), and finally, all Aβ$_{1-42}$ and CTF peptides in each trajectory converged into a single large heterotypic assembly (Fig. 1d–e). These results are in qualitative agreement with the DLS observations of increased abundance of Aβ$_{1-42}$ oligomers in the presence of these CTFs relative to Aβ$_{1-42}$ alone.[35] Thus, the three toxicity inhibitors (Aβ$_{30-40}$, Aβ$_{31-42}$, or Aβ$_{39-42}$) acted as a "glue" capturing Aβ$_{1-42}$ molecules into an amorphous heterotypic assembly. In contrast, the control peptide Aβ$_{21-30}$ had the opposite effect. In the presence of this fragment, both Aβ$_{1-42}$ and Aβ$_{21-30}$ remained predominantly monomeric. In addition, small heterotypic assemblies comprising

an Aβ$_{1-42}$ molecule surrounded by seven to eight Aβ$_{21-30}$ peptides also were observed (Fig. 2a–e, see also Fig. II in Supplementary Material). The size distributions of Aβ$_{1-42}$/Aβ$_{X-Y}$ assemblies (Fig. II in Supplementary Material) evolved within 5×10^6 to 10×10^6 simulation steps into a quasi-steady state, after which the temporal changes in the oligomer size distributions were no longer statistically significant up to 20×10^6 simulation steps.

CTFs inhibit β-strand formation in Aβ$_{1-42}$

The structural basis for Aβ$_{1-42}$ neurotoxicity is as yet unknown. Several studies addressed the relevance of β-strand formation in Aβ-oligomer-mediated toxicity. Neurotoxic pre-fibrillar Aβ assemblies lacking the cross-β structure (which is characteristic of Aβ fibrils with ~45–55% of β-sheet structure) were identified by several studies.[13,19,45,46] In contrast, Chimon *et al.* described neurotoxic Aβ intermediates with parallel β-sheet structures,[47] and Wu *et al.* found fibrillar oligomers that nucleated formation of toxic oligomers but did not form fibrils.[48] Our DMD-derived oligomer structures[25] are consistent with *in vitro* data by Kirkitadze *et al.* who found Aβ$_{1-40}$ and Aβ$_{1-42}$ oligomers with a relatively low β-strand of 10–20%[45] and no cross-β structure. Here, we asked whether changes in the β-strand propensity in Aβ$_{1-42}$ due to the presence of CTFs and Aβ$_{21-30}$ at the stage of initial hydrophobic collapse may correlate with their reported ability to inhibit Aβ$_{1-42}$ toxicity.

To examine the effect of Aβ fragments on β-strand formation in Aβ$_{1-42}$, we calculated the average β-strand content, ⟨β-strand⟩, of Aβ$_{1-42}$ within Aβ$_{1-42}$/Aβ$_{X-Y}$ assemblies and compared them to ⟨β-strand⟩ in Aβ$_{1-42}$ oligomers formed in the absence of fragments (Fig. 3a, continuous curves). ⟨β-Strand⟩ in Aβ$_{1-42}$ decreased from 19% in the absence of fragments to ~16% at relative molar concentrations of Aβ$_{X-Y}$ of ~0.5 for all toxicity inhibitors. At the relative Aβ$_{X-Y}$ molar concentrations of ~1, Aβ$_{30-40}$ and Aβ$_{31-42}$ further reduced ⟨β-strand⟩ in Aβ$_{1-42}$ to ~15%. At this Aβ$_{31-42}$ concentration, ⟨β-strand⟩ in Aβ$_{1-42}$ was at its lowest value, and at the relative Aβ$_{31-42}$ molar concentration above 2 and up to 10, ⟨β-strand⟩ remained at a value of ~16% (~16% reduction). ⟨β-Strand⟩ in Aβ$_{1-42}$ above the relative Aβ$_{30-40}$ molar concentration of ~2 decreased with the Aβ$_{30-40}$ concentration and reached a value of ~12% at the relative molar concentration of 10 (37% reduction). Thus, of the two longer toxicity inhibitors, Aβ$_{30-40}$ was significantly more efficient in suppressing the formation of β-strand structure in Aβ$_{1-42}$ than Aβ$_{31-42}$. The shortest toxicity inhibitor, Aβ$_{39-42}$, had the most prominent effect on ⟨β-strand⟩ in Aβ$_{1-42}$ at all relative molar concentrations >0.5 and reduced ⟨β-strand⟩ to ~10% (48% reduction). In contrast to the three toxicity inhibitors, the control
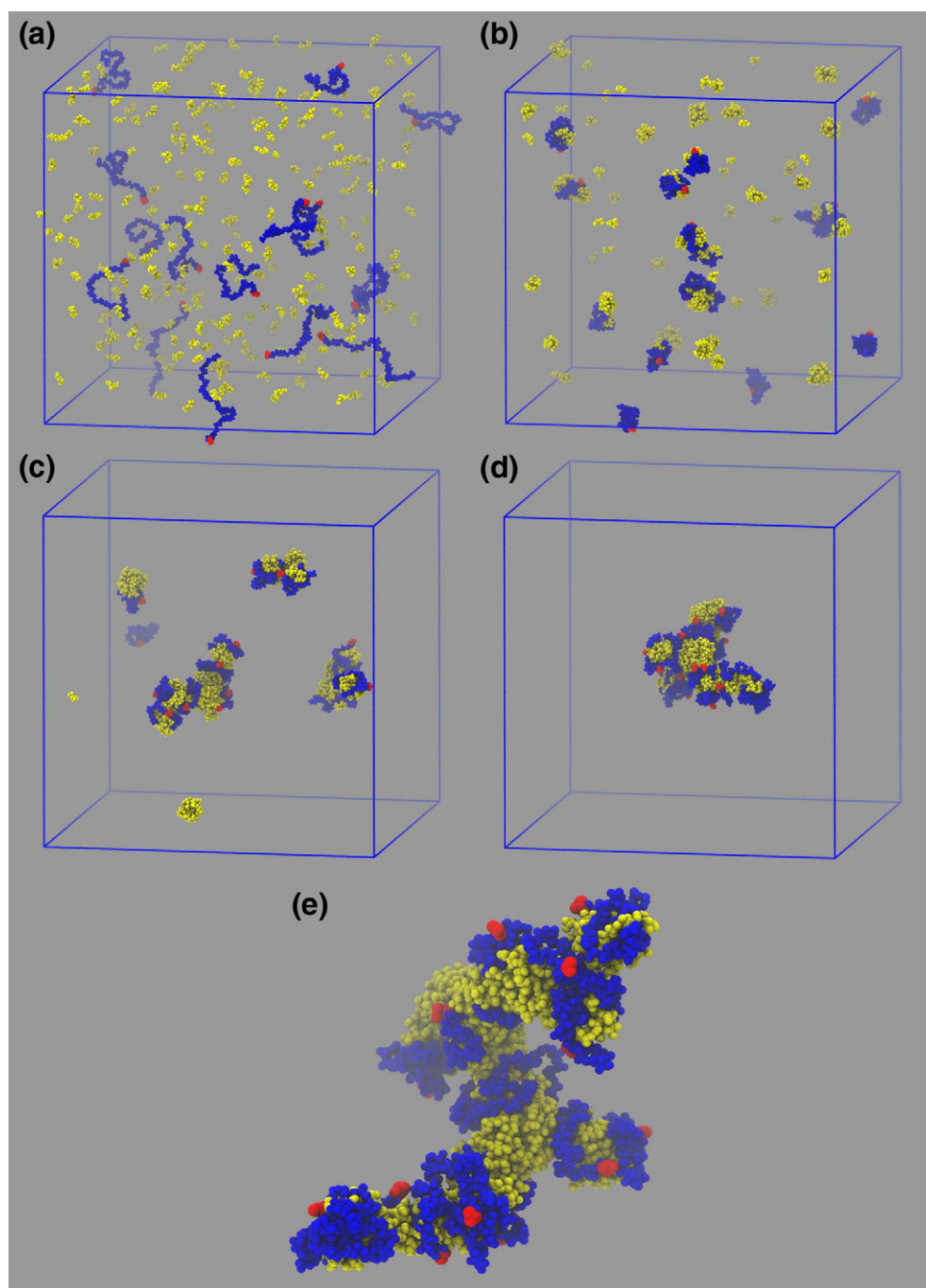
Fig. 1. Populations of 16 Aβ$_{1-42}$ and (a–d) 256 Aβ$_{39-42}$ molecules at four different time frames: (a) $t = 0$ (b), $t = 0.1 \times 10^6$, $t = 10^6$, and $t = 20 \times 10^6$ simulation steps. Aβ$_{39-42}$ molecules are displayed in yellow, and Aβ$_{1-42}$ molecules are represented in dark blue with the N-terminal amino acid D1 marked as red spheres. (e) A magnified and rotated final Aβ$_{1-42}$/Aβ$_{39-42}$ heterooligomer obtained at $t = 20 \times 10^6$ simulation steps. The figure was created using the VMD software package.[44]

peptide Aβ$_{21-30}$ increased ⟨β-strand⟩ in Aβ$_{1-42}$ (Fig. 3a, gray continuous curve), and this increase was strongly Aβ$_{21-30}$ concentration dependent.

⟨β-Strand⟩ propensity in the Aβ fragments themselves was variable. All three toxicity inhibitors showed similar concentration dependencies of ⟨β-strand⟩ (Fig. 3a, black, red, and green broken curves), experiencing a slight Aβ$_{1-42}$-induced increase in ⟨β-strand⟩ about or just below the relative molar CTF concentrations of 0.5, followed by a decrease at higher CTF concentrations. Aβ$_{31-42}$ had the highest ⟨β-strand⟩ values at all concentrations under study, reaching ~12% at the highest relative Aβ$_{31-42}$ molar concentration of 10, followed by
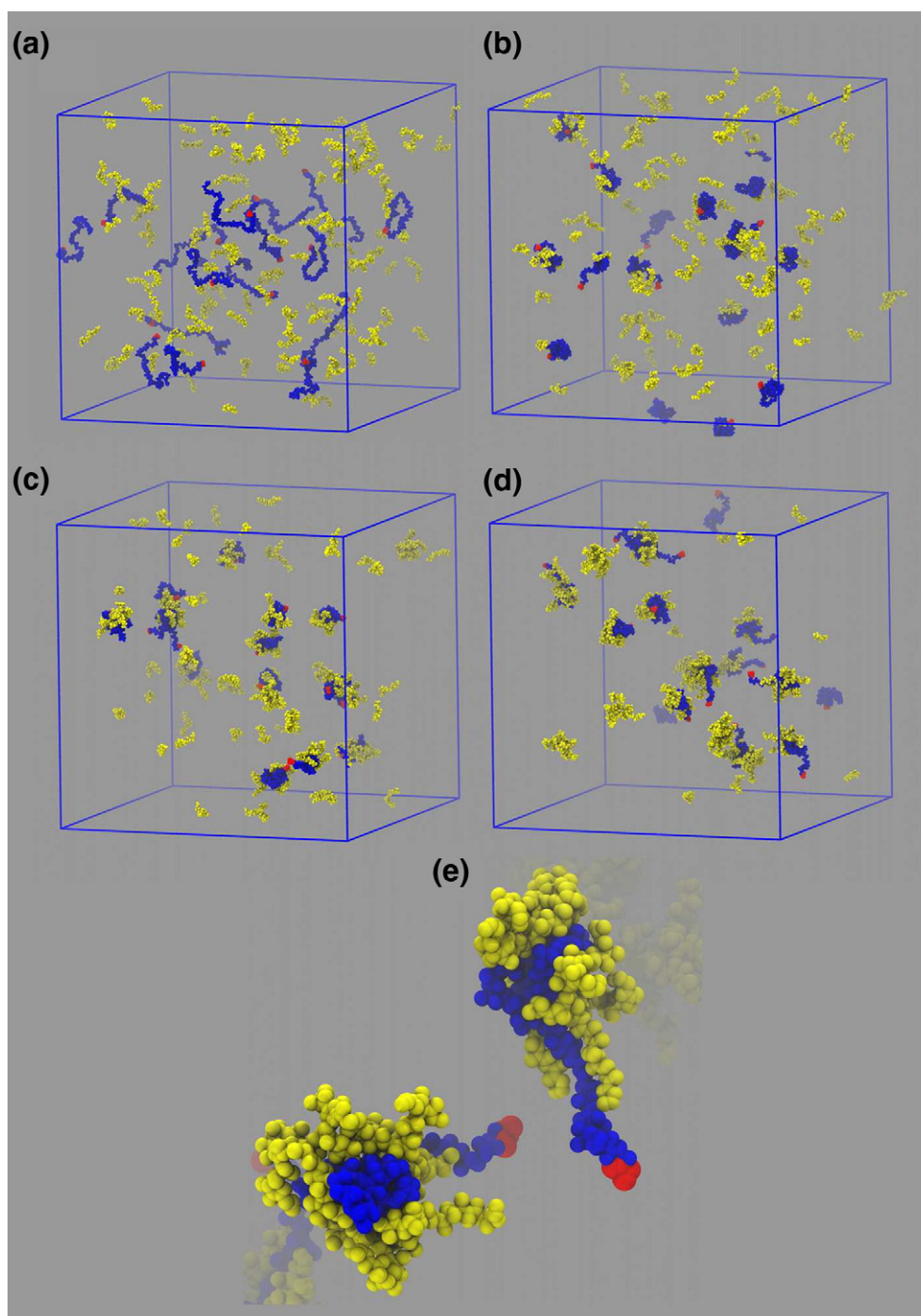
Fig. 2. Populations of 16 Aβ$_{1-42}$ and (a–d) 128 Aβ$_{21-30}$ molecules at four different time frames: (a) $t = 0$ (b), $t = 0.1 \times 10^6$, $t = 10^6$, and $t = 20 \times 10^6$ simulation steps. Aβ$_{21-30}$ molecules are displayed in yellow, and Aβ$_{1-42}$ molecules are represented in dark blue with the N-terminal amino acid D1 marked as red spheres. (e) Two magnified Aβ$_{1-42}$/Aβ$_{21-30}$ heterooligomers obtained at $t = 20 \times 10^6$ simulation steps. The figure was created using the VMD software package.[44]

Aβ$_{30-40}$ with ∼7% and Aβ$_{39-42}$ with ∼2%. The control peptide Aβ$_{21-30}$ was characterized by the highest ⟨β-strand⟩ (ranging from 12.8% at the lowest to 17.6% at the highest Aβ$_{21-30}$ concentration) of all four Aβ fragments. ⟨β-Strand⟩ in Aβ fragments was at all concentrations lower than ⟨β-strand⟩ in Aβ$_{1-42}$ oligomers formed in the absence of fragments (19.1%) and significantly lower than that of Aβ$_{1-42}$ assembling in the presence of Aβ$_{21-30}$ at the 1:10 molar concentration ratio (27.9%). As shown in
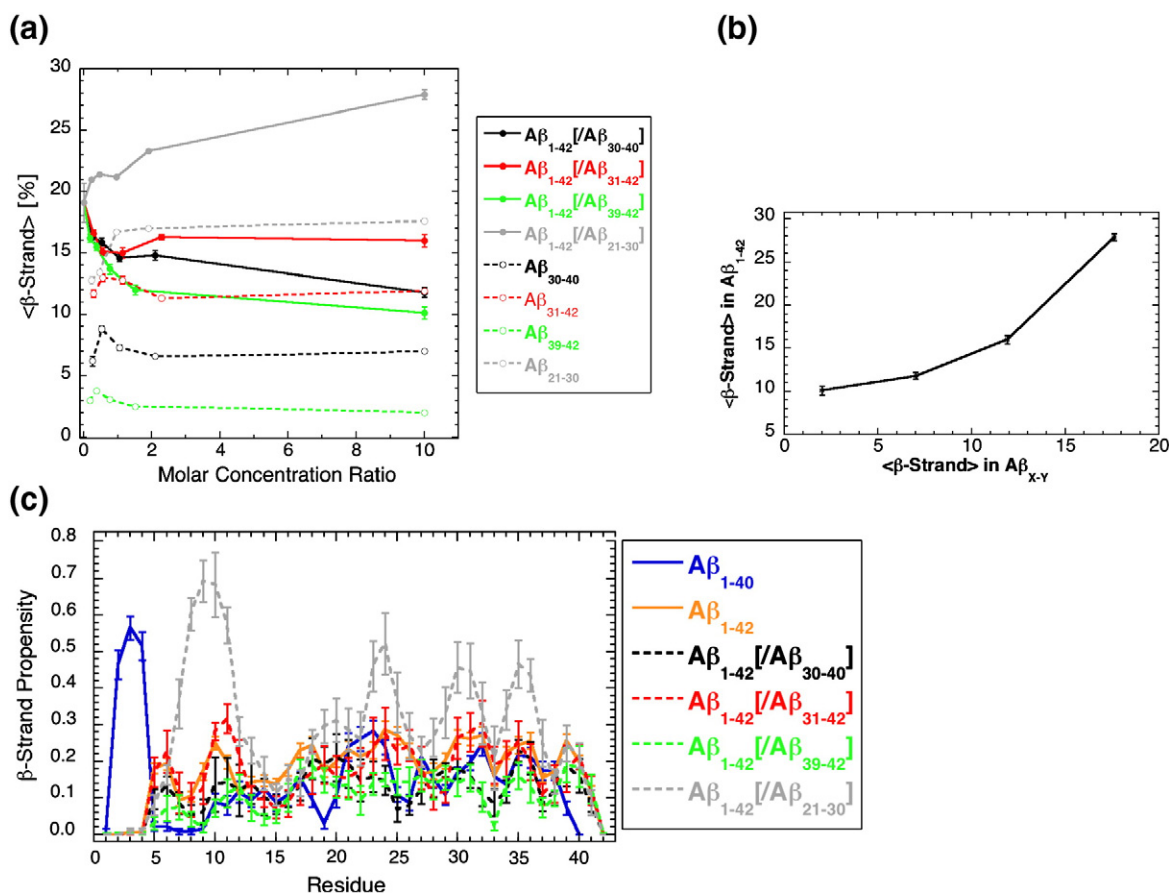
Fig. 3. (a) Average β-strand of $A\beta_{1-42}$ (continuous lines) *versus* the relative molar concentration of each Aβ fragment: $A\beta_{30-40}$ (black lines), $A\beta_{31-42}$ (red lines), $A\beta_{39-42}$ (green lines), or $A\beta_{21-30}$ (gray lines) as well as the average β-strand propensities of Aβ fragments within heterooligomers (broken lines). Heterooligomer populations of 11 time frames between 19×10^6 and 20×10^6 simulation steps of each of eight trajectories per concentration and per the CTF type were used in the analysis. (b) The average β-strand propensity in $A\beta_{1-42}$ as a function of the average β-strand propensity in the Aβ fragment. (c) β-Strand propensity per residue. The error bars correspond to standard error of the mean.

Fig. 3b, the β-strand propensity of Aβ fragments correlated with the average β-strand in $A\beta_{1-42}$ and also with the Aβ-fragment-induced change in the $A\beta_{1-42}$ β-strand propensity. To our knowledge, there are currently no experimental data on the effect of Aβ fragments on the secondary structure of $A\beta_{1-42}$; thus, direct comparison between *in silico* and *in vitro* data cannot be made. Nonetheless, our analysis suggests that the $A\beta_{1-42}$ secondary structure changes may be relevant to the Aβ-fragment-induced changes in $A\beta_{1-42}$ toxicity.

In addition, we compared β-strand propensities per residue in $A\beta_{1-40}$ and $A\beta_{1-42}$ hexamers formed in the absence of fragments (Fig. 3c, blue and orange curves) with the β-strand propensities per residue in heterotypic assemblies comprising $A\beta_{1-42}$ and Aβ fragments (Fig. 3c, black, red, green, and gray curves). None of the three toxicity inhibitors changed the relative distribution of β-strand propensities along the $A\beta_{1-42}$ sequence. The β-strand

propensity per residue in $A\beta_{1-42}$ hexamers was significantly different from the one found in $A\beta_{1-40}$ hexamers, as reported and discussed in our prior work.[25] For example, region A2–F4 in $A\beta_{1-40}$ but not in $A\beta_{1-42}$ hexamers had a high β-strand propensity (Fig. 3c, blue and orange curves). All three toxicity inhibitors reduced the β-strand propensities in region Q15–L17 of $A\beta_{1-42}$, but only $A\beta_{30-40}$ and $A\beta_{39-42}$ reduced these propensities at R5–V12, A21–S26, and I31–V36. The control peptide $A\beta_{21-30}$, on the other hand, substantially increased the β-strand propensity in several $A\beta_{1-42}$ regions: D7–E11, F19–F20, E22–V24, G29–I32, and L34–V36 (Fig. 3c, gray curve).

Aβ$_{X–Y}$ fragments alter the tertiary and quaternary structures of Aβ$_{1–42}$

Here, we quantified structural changes in $A\beta_{1-42}$ due to the presence of each fragment and identified

the specific peptide regions involved in the interaction between Aβ$_{1-42}$ and Aβ$_{X-Y}$. For this purpose, simulation data corresponding to the Aβ$_{1-42}$/Aβ$_{X-Y}$ molar concentration ratio 1:10, which was needed for an efficient toxicity inhibition, were used‡.[32] In these simulations, six Aβ$_{1-42}$ molecules co-assembled with 229 Aβ$_{30-40}$, 210 Aβ$_{31-42}$, 630 Aβ$_{39-42}$, or 252 Aβ$_{21-30}$ peptides using a simulation box size of 318 Å.

Effect of Aβ fragments on the tertiary structure of Aβ$_{1-42}$

The tertiary structures of Aβ$_{1-42}$ in the absence or presence of Aβ fragments are shown in Fig. 4a–e. All three toxicity inhibitors slightly reduced the number and strength of intramolecular contacts relative to Aβ$_{1-42}$ hexamers formed in the absence of inhibitors, mostly in the N-terminal region (Fig. 4a–e, box 1). Almost no change in the tertiary structure was observed at the C-terminal region (Fig. 4a–e, box 4). Among the three inhibitors, Aβ$_{39-42}$ reduced the intramolecular contacts in Aβ$_{1-42}$ the most (Fig. 4d). The control peptide Aβ$_{21-30}$ inhibited the Aβ$_{1-42}$ intramolecular contacts at the N-terminal region (Fig. 4e, box 1) but, at the same time, increased the number and strengths of intramolecular contacts in all other regions of Aβ$_{1-42}$ (Fig. 4e, boxes 2–5) relative to Aβ$_{1-42}$ hexamers (Fig. 4a). Overall, the three CTFs decreased—whereas Aβ$_{21-30}$ increased—the stability of the Aβ$_{1-42}$ tertiary structure. The exception was the N-terminal region (Fig. 4a–e, box 1), where all Aβ$_{X-Y}$ reduced intramolecular contacts in Aβ$_{1-42}$.

Effect of Aβ fragments on the quaternary structure of Aβ$_{1-42}$

The quaternary structures of Aβ$_{1-42}$ in the absence or presence of Aβ fragments are shown in Fig. 4f–j. All four Aβ fragments reduced both the number and the strengths of intermolecular contacts among Aβ$_{1-42}$ molecules in a concentration-dependent way (Fig. IV, Supplementary Material). The remaining intermolecular Aβ$_{1-42}$ contacts were Aβ$_{X-Y}$ specific. An almost complete absence of specific intermolecular contacts among Aβ$_{1-42}$ was observed in the presence of Aβ$_{30-40}$ and Aβ$_{21-30}$. The interpretation of this reduction was, however, different for the two peptides. In the case of Aβ$_{21-30}$, Aβ$_{1-42}$ molecules did not interact because they belonged to different heterotypic assemblies, whereas in the case of Aβ$_{30-40}$, all six Aβ$_{1-42}$

---

‡A similar structural analysis for Aβ$_{1-42}$ and Aβ fragments using simulation data obtained at the four lower Aβ$_{1-42}$/Aβ$_{X-Y}$ concentration ratios is described in Supplementary Results in Supplementary Material (Figs. III–VII).

molecules belonged to the same Aβ$_{1-42}$/Aβ$_{30-40}$ heterooligomer but were spatially separated from each other, resulting in the reduction in all intermolecular contacts. Similar to Aβ$_{30-40}$, Aβ$_{31-42}$ and Aβ$_{39-42}$ spatially separated individual Aβ$_{1-42}$ molecules within heterooligomers. Interestingly, none of the four fragments completely inhibited the intermolecular Aβ$_{1-42}$ contacts. In the presence of Aβ$_{31-42}$ or Aβ$_{39-42}$, the intermolecular contacts among Aβ$_{1-42}$ molecules were more abundant than in the presence of Aβ$_{30-40}$. In the presence of Aβ$_{39-42}$, the intermolecular contacts among the CHC, MHR, and CTR regions of Aβ$_{1-42}$ were more abundant than in the presence of Aβ$_{31-42}$. Aβ$_{31-42}$ induced a few new intermolecular contacts involving the N-terminal region G9–V12 of Aβ$_{1-42}$ (Fig. 4h, box 5).

Interaction regions between Aβ$_{1-42}$ and Aβ fragments

Intermolecular contacts between Aβ$_{1-42}$ and each fragment are shown in Fig. 4k–n. Boxes 1–4 indicate the regions of Aβ$_{1-42}$ that most strongly interacted with all four fragments: the A2–F4 region, CHC, MHR, and CTR. Of the four fragments, Aβ$_{39-42}$ formed the most frequent contacts with Aβ$_{1-42}$, likely due to its highly hydrophobic nature and its short length (Fig. 4m). Aβ$_{30-40}$ and Aβ$_{31-42}$ displayed comparable average numbers and strengths of intermolecular contacts (Fig. 4k and l), though the strengths were slightly increased in Aβ$_{30-40}$ relative to Aβ$_{31-42}$. The intermolecular contacts between the control Aβ$_{21-30}$ peptide and Aβ$_{1-42}$ were comparable to those observed for Aβ$_{30-40}$ and Aβ$_{31-42}$ in CHC, MHR, and CTR (Fig. 4n, boxes 2–4). There were no contacts between Aβ$_{21-30}$ and the A2–F4 region of Aβ$_{1-42}$ (Fig. 4n, box 1). Instead, region R5–V12 of Aβ$_{1-42}$ formed an antiparallel β-sheet with Aβ$_{21-30}$ (Fig. 4n, region between boxes 1 and 2). These contacts were specific to Aβ$_{21-30}$ interaction with Aβ$_{1-42}$ and were not observed for any other Aβ fragment. Thus, the interaction between Aβ$_{21-30}$ and Aβ$_{1-42}$ was stronger than would have been expected based on the strongly hydrophilic nature of Aβ$_{21-30}$ relative to CTFs.

Binding propensity of Aβ$_{X-Y}$ to Aβ$_{1-42}$

To quantify the degree of the interaction between Aβ$_{1-42}$ and Aβ$_{X-Y}$, we calculated the binding propensity by averaging the intermolecular Aβ$_{1-42}$/Aβ$_{X-Y}$ contact maps shown in Fig. 4k–n over the specified regions. The results are shown in Table 1. For comparison, the binding propensity of Aβ$_{1-42}$ to itself in hexamers was included. We found that Aβ$_{39-42}$ had ∼2- to 4-fold higher binding propensity than the other three fragments to the four regions of Aβ$_{1-42}$ under study (Table 1). Aβ$_{21-30}$ had a binding propensity
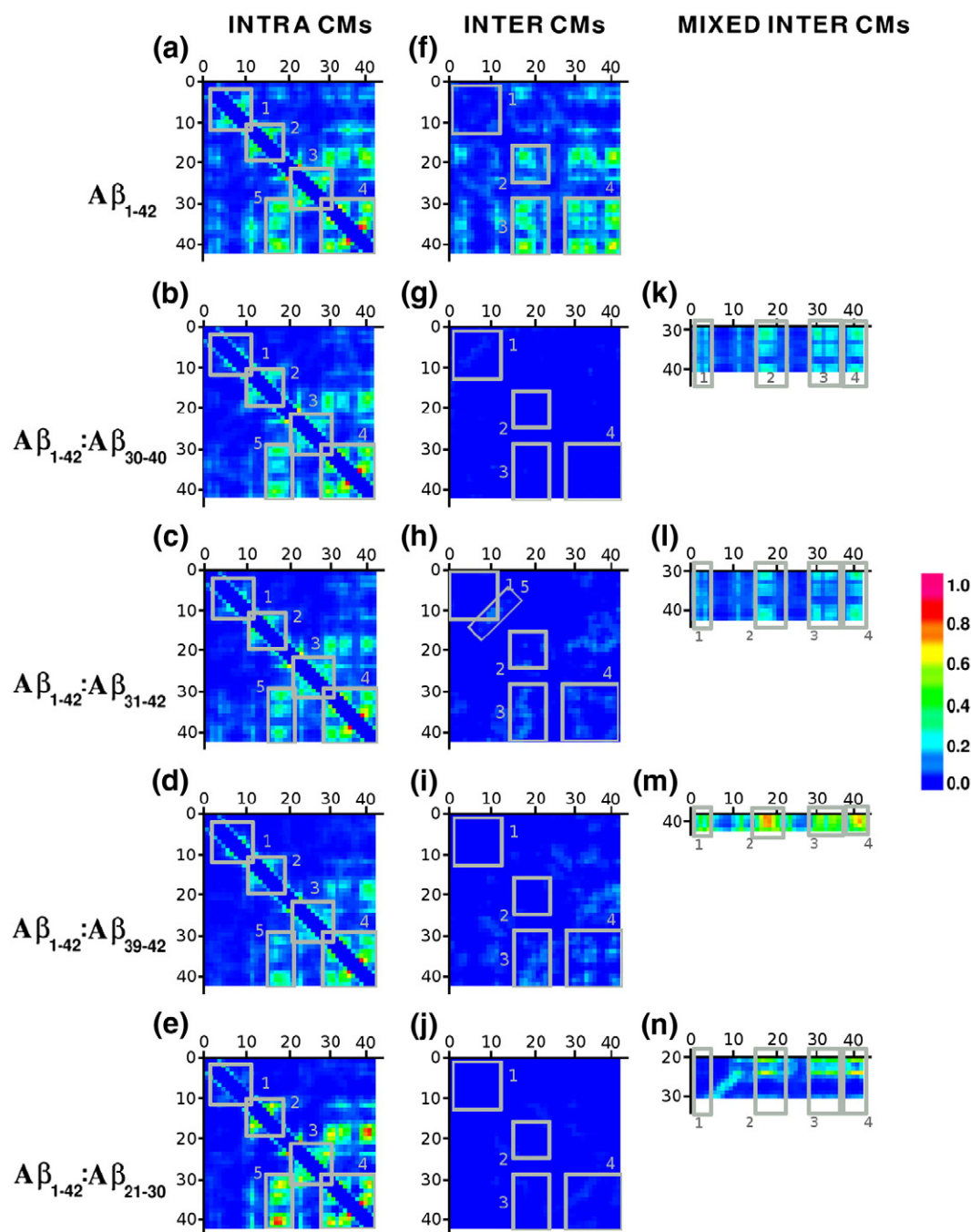
Fig. 4. Intramolecular (a–e) and intermolecular (f–j) contact maps of Aβ$_{1-42}$ assemblies formed in the absence and at 1:10 molar concentration ratio of the three toxicity inhibitors (Aβ$_{30-40}$, Aβ$_{31-42}$, and Aβ$_{39-42}$) and the control peptide Aβ$_{21-30}$. The intramolecular and intermolecular contact maps of Aβ$_{1-42}$ hexamers are shown in (a) and (f), respectively. The intermolecular maps that elucidate regions of contact between Aβ$_{1-42}$ and each of the four Aβ fragments are shown in (k) to (n). The contact maps are oriented such that the average number of contacts among the N-terminal amino acids is displayed at the top left corner and the average number of contacts among the C-terminal amino acids is at the bottom right corner. The boxes mark regions of concentrated contacts.

similar to that of CHC, MHR, and CTR as Aβ$_{30-40}$ and Aβ$_{31-42}$ despite its predominant hydrophilic nature. Importantly, Aβ$_{21-30}$ had at least 5-fold lower binding propensity to the A2–F4 region of Aβ$_{1-42}$ relative to the CTFs, highlighting a possible relevance of the A2–F4 region of Aβ$_{1-42}$ in mediating toxicity.

Table 1. Binding propensity of Aβ$_{30-40}$, Aβ$_{31-42}$, Aβ$_{39-42}$, and Aβ$_{21-30}$ to specific regions of Aβ$_{1-42}$ at an Aβ$_{1-42}$/Aβ$_{X-Y}$ molar concentration ratio of 1:10

Aβ$_{1-42}$ regions	Aβ$_{30-40}$	Aβ$_{31-42}$	Aβ$_{39-42}$	Aβ$_{21-30}$	Aβ$_{1-42}$ hexamers
A2–F4	0.59 ± 0.03	0.51 ± 0.03[a]	1.69 ± 0.19[b]	0.09 ± 0.02[c]	0.07 ± 0.01
CHC	0.66 ± 0.04	0.65 ± 0.03	2.45 ± 0.16[b]	0.64 ± 0.09	0.14 ± 0.01
MHR	0.70 ± 0.04	0.57 ± 0.03[a]	1.89 ± 0.13[b]	0.62 ± 0.09	0.15 ± 0.01
CTR	0.74 ± 0.05	0.72 ± 0.05	2.27 ± 0.18[b]	0.74 ± 0.14	0.18 ± 0.01

Binding propensities of Aβ$_{1-42}$ to itself in unaltered Aβ$_{1-42}$ hexamers are given for comparison.
 [a] Aβ$_{31-42}$ binding propensities that were significantly different from Aβ$_{30-40}$ binding propensities (nonoverlapping error bars).
 [b] Aβ$_{39-42}$ binding propensities that were two to four times larger than those for any other fragment.
 [c] Aβ$_{21-30}$ binding propensity to the A2–F4 region more than five times lower than that for any other fragment. The error bars correspond to standard error of the mean.

CTFs reduce solvent exposure of the N-terminal region of Aβ₁₋₄₂

Aβ$_{1-42}$ oligomers presumably mediate neurotoxicity through interaction with cell membranes and/or other cellular components.[49–52] Important insights into the specific Aβ$_{1-42}$ regions participating in these interactions may be gleaned from studying which regions are most exposed to the environment within homotypic and heterotypic assemblies. In our recent study, we showed that the solvent-accessible surface area (SASA) in the N-terminal region was significantly lower in Aβ$_{1-40}$ hexamers than in Aβ$_{1-42}$ hexamers (see Fig. S5b in Supporting Information of Ref. 25). To check whether this difference between Aβ$_{1-40}$ and Aβ$_{1-42}$ was specific to hexamers or a more general feature, we used here data from our previous study[25] to calculate SASA per residue using the entire Aβ$_{1-40}$ and Aβ$_{1-42}$ populations of monomers and oligomers. The results demonstrated that the distinct SASA profiles in the N-terminal region D1–R5 between Aβ$_{1-40}$ and Aβ$_{1-42}$ were characteristic not only for hexamers but also for entire Aβ$_{1-40}$ and Aβ$_{1-42}$ populations (Fig. 5, blue and orange curves). The regions of Aβ that on average were most exposed to the solvent were mostly hydrophilic residues (D1, R5–S8, H13–Q15, E22–D23, and S26–K28), whereas the hydrophobic regions (CHC, MHR, and CTR) had low SASA values.

To quantify the effect of Aβ fragments on the solvent exposure of Aβ$_{1-42}$, we calculated SASA per residue using the simulation data acquired at the Aβ$_{1-42}$/Aβ$_{X-Y}$ molar concentration ratio 1:10 (Fig. 5). For Aβ$_{1-42}$ assembled in the presence of the three toxicity inhibitors, the SASA in region D1–R5 was reduced relative to Aβ$_{1-42}$ assembled in the absence of inhibitors. For all three CTFs, the SASA values almost overlapped with the SASA values derived for Aβ$_{1-40}$ assemblies formed in the absence of Aβ fragments (Fig. 5). In contrast, Aβ$_{21-30}$ induced an increased SASA in region D1–R5 of Aβ$_{1-42}$ (Fig. 5, gray curve). The observed correlation between solvent exposure of the N-terminal region of Aβ$_{1-42}$ and the degree of toxicity suggests that the N-terminal region D1–R5 of Aβ$_{1-42}$ is involved in Aβ$_{1-42}$-mediated toxicity, likely through interaction with cellular targets.

Discussion

Our recent *in vitro* studies of a series of CTFs (Aβ$_{X-42}$, X = 29–39; Aβ$_{30-40}$) and the control peptide Aβ$_{21-30}$ were studied for aqueous solubility, aggregation propensity, and morphology
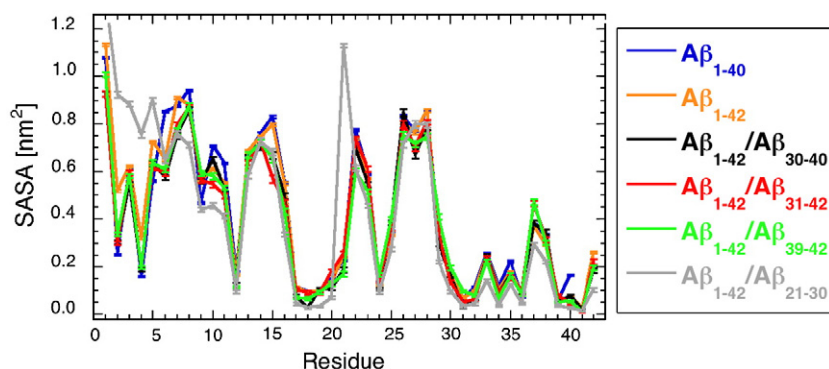

Fig. 5. Average SASA per residue of Aβ$_{1-40}$ and Aβ$_{1-42}$ monomer and oligomer populations assembled in the absence and presence of the three CTFs at the molar concentration ratio 1:10, relevant to toxicity inhibition, and the control peptide Aβ$_{21-30}$ at the same molar concentration ratio.

characteristics. None of these properties directly correlated with the ability of CTFs to inhibit toxicity.[33] Rather, the degree of toxicity inhibition by CTFs, in particular, $A\beta_{31-42}$, $A\beta_{39-42}$, and $A\beta_{30-40}$, correlated with stabilization of the smaller and attenuation of the larger of the two oligomer populations with hydrodynamic radii of 8–12 nm and 20–60 nm, respectively, as measured by DLS.[35] These findings are difficult to reconcile using a simple explanation of how the inhibitors affect $A\beta_{1-42}$ assembly but, rather, demonstrate that (i) CTFs do not prevent $A\beta_{1-42}$ self-assembly, (ii) CTFs bind to $A\beta_{1-42}$ and subtly affect its assembly, and (iii) CTFs and $A\beta_{1-42}$ co-assemble into oligomeric structures that are not grossly different from those formed in the absence of inhibitors (i.e., they have similar hydrodynamic radii[35] and similar morphologies) (H.L. and G.B., unpublished results).

Two plausible mechanisms by which inhibitors could reduce $A\beta_{1-42}$ toxicity are as follows: (a) CTFs modulate $A\beta_{1-42}$ oligomer structure by inducing subtle structural changes or (b) CTFs mask $A\beta_{1-42}$ groups or regions that interact with cellular targets. These mechanisms are not mutually exclusive and may be operating together. Our purpose in the present study was to gain insight into these mechanisms from the relatively high resolution data provided by the DMD approach. Thus, we examined the structures and structural changes occurring during early stages of $A\beta_{1-42}$ assembly in the presence of three selected toxicity inhibitors ($A\beta_{30-40}$, $A\beta_{31-42}$, and $A\beta_{39-42}$) or a control peptide ($A\beta_{21-30}$). $A\beta_{1-42}$ was found to co-assemble with all three CTFs under study into large heterooligomers. In contrast, $A\beta_{1-42}$ and $A\beta_{21-30}$ formed small heterotypic assemblies comprising mostly one $A\beta_{1-42}$ and seven to eight $A\beta_{21-30}$ peptides. Thus, in our simulations, toxicity inhibitors but not control peptides induced formation of large heterooligomers.

Mechanisms by which toxicity inhibitors interact with Aβ to reduce toxicity are not well understood. Liu *et al.* showed that a simple disaccharide, trelahose, inhibited oligomer formation and reduced toxicity of $A\beta_{1-40}$ but not that of $A\beta_{1-42}$.[53] This study suggests that trelahose induced alloform-specific structural changes that disrupted specific interactions of $A\beta_{1-40}$, but not those of $A\beta_{1-42}$, with its environment. Similarly, here, we found specific interactions of different inhibitors with $A\beta_{1-42}$. Though all three CTFs decreased the tendency of $A\beta_{1-42}$ to form β-strands, $A\beta_{39-42}$ was the most efficient and $A\beta_{31-42}$, the least efficient among the three. The ability to disrupt β-strand formation was negatively correlated with the β-strand content in CTFs themselves. In contrast to CTFs, $A\beta_{21-30}$ significantly increased the propensity of $A\beta_{1-42}$ to form the β-strands.

Of the four Aβ fragments, $A\beta_{39-42}$ interacted most strongly with $A\beta_{1-42}$. Interestingly, the predominantly hydrophilic $A\beta_{21-30}$ interacted with $A\beta_{1-42}$ as strongly as $A\beta_{30-40}$ or $A\beta_{31-42}$, though the location and nature of these interactions were distinct from those between $A\beta_{1-42}$ and the two CTFs. These results suggest that peptide length affects the $A\beta_{1-42}/A\beta_{X-Y}$ interaction more than does its hydrophobic *versus* hydrophilic nature. As expected, the self-assembly of $A\beta_{X-Y}$ was strongly affected by the hydrophobic *versus* hydrophilic character of the fragments. In contrast to the CTFs, $A\beta_{21-30}$ did not self-assemble. Importantly, unlike the three toxicity inhibitors, $A\beta_{21-30}$ did not interact with the A2–F4 region of $A\beta_{1-42}$.

An involvement of the A2–F4 region in $A\beta_{1-40}$ but not $A\beta_{1-42}$ folding and oligomer formation was demonstrated in previous DMD studies.[22,24,25] In $A\beta_{1-40}$, the A2–F4 region had a relatively high β-strand propensity,[22,24,25] resulting in less favorable $A\beta_{1-40}$ hexamer formation, which included a slow dock-and-lock intermolecular interaction involving the A2–F4 β strand regions.[25] Intermolecular contacts among the A2–F4 regions caused the N-terminal region to be more shielded from the solvent in $A\beta_{1-40}$ than in $A\beta_{1-42}$ oligomers.

Similar to the differences between $A\beta_{1-40}$ and $A\beta_{1-42}$, our present analysis showed that region D1–R5 of $A\beta_{1-42}$ was significantly less exposed to the solvent in heterooligomers formed in the presence of toxicity inhibitors than in $A\beta_{1-42}$ oligomers formed in the absence of Aβ fragments. In contrast, in the presence of $A\beta_{21-30}$, the solvent exposure of the N-terminal region D1–R5 of $A\beta_{1-42}$ significantly increased relative to unaltered $A\beta_{1-42}$ oligomers.

Our hypothesis that the N-terminus of $A\beta_{1-42}$ mediates $A\beta_{1-42}$-induced toxicity is consistent with findings of two recent studies. Luheshi *et al.* who used a *Drosophila* model of AD demonstrated that (a) an A2F substitution in $A\beta_{1-42}$ increased its toxicity, and (b) whereas an E22G substitution in $A\beta_{1-42}$ dramatically increased its toxicity, a double substitution, E22G/F4D, led to a significantly reduced toxicity.[54] In addition, Jin *et al.* used Aβ dimers isolated from the cortex of AD patients and showed that they mediate toxicity by directly inducing Tau phosphorylation. They further demonstrated that the monoclonal antibodies that bind to the N-terminal D1, but not the antibody that binds to the C-terminus of $A\beta_{1-42}$, inhibited this Aβ-mediated toxicity.[55]

In summary, our present results offer mechanistic insights into processes involved in $A\beta_{1-42}$ assembly in the presence of Aβ fragments and provide an insight into the putative mechanism(s) by which the CTFs inhibit toxicity. We identified two structural elements, increased β-strand propensity and increased solvent exposure at the N-terminus of $A\beta_{1-42}$, that correlated with $A\beta_{1-42}$-induced toxicity

Table 2. Summary of the cell viability data for Aβ₁₋₄₂-induced toxicity in cell cultures extracted from Fradinger *et al.*[32] and for Aβ₁₋₄₂ in the presence of Aβ fragments extracted from Li *et al.*[33] (column 2) alongside the main structural changes in Aβ₁₋₄₂ during its assembly at the highest concentration of Aβ fragments as observed here (columns 3–5)

Aβ$_{X-Y}$	Cell viability (%)	Assembly state	Δ⟨β-strand⟩ (%)	ΔSASA
Aβ$_{1-42}$	62 ± 4	Oligomers	0	≡0
+ Aβ$_{30-40}$	98 ± 7	Large H-O	−7	<0
+ Aβ$_{31-42}$	105 ± 5	Large H-O	−3	<0
+ Aβ$_{39-42}$	89 ± 5	Large H-O	−9	<0
+ Aβ$_{21-30}$	63 ± 7	Ms/small H-Os	9	>0

H-O, heterooligomer; M, monomer.

(Table 2). This work delineates plausible structure–toxicity relationships amenable to *in vitro* and *in vivo* testing and provides structural information of potential importance for drug design.

Methods

The DMD approach

DMD is a form of molecular dynamics that utilizes interparticle potentials in a form of a single or a combination of square wells, which simplifies calculations of individual trajectories and makes DMD orders of magnitude faster than molecular dynamics.[56] Here, DMD is combined with a four-bead protein model, in which each amino acid is described by up to four beads (representing the amino N, α-carbon C^α, carboxyl C, and β-carbon C^β groups).[57,58] This four-bead protein model is based on geometric properties and the backbone hydrogen bonding introduced by Ding *et al.*[58] The lengths of bonds and the angular constraints are determined phenomenologically by calculating their distributions using the known folded protein structures of ∼7700 proteins from the Protein Data Bank.[58,59] Effective backbone hydrogen bonds are implemented between the nitrogen atom N$_i$ of the *i*-th amino acid and the carbon atom C$_j$ of the *j*-th amino acid.[58] The absolute value of the potential energy of the backbone hydrogen bond interaction, E_{HB}, represents a unit of energy, and the temperature is given in units of E_{HB}/k_B. We implemented the amino-acid-specific interactions due to hydropathy and charge of individual side chains that are critical[21] to distinguish between Aβ₁₋₄₀ and Aβ₁₋₄₂ folding and assembly pathways.[20,22,25] The *ab initio* DMD approach with a four-bead protein model and implicit solvent used in this study is the same as that used in the previous studies of Aβ folding and assembly[22–25] and has been described in detail by Urbanc *et al.*[20] Relative to earlier DMD studies,[22,23,32] a present DMD parametrization includes a more accurate estimate of physiological temperature and two times longer simulation time, which was recently shown to best account for the distinct oligomer size distributions of Aβ₁₋₄₀, Aβ₁₋₄₂, and their Arctic mutants.[24,25]

The DMD simulation protocol

Keeping the number of Aβ₁₋₄₂ molecules fixed (either 16 or 6), we varied the number of Aβ$_{X-Y}$ molecules to obtain a desired Aβ₁₋₄₂/Aβ$_{X-Y}$ concentration ratio. The total molar concentration was kept constant across simulations and equal to the one used in our previous study of oligomer formation of full-length Aβ peptides.[25] Initially, the centers of mass of unstructured monomeric Aβ₁₋₄₂ and Aβ$_{X-Y}$ molecules were arranged in the simulation box into a cubic lattice. Distinct initial configurations for multiple trajectories per each Aβ₁₋₄₂/Aβ$_{X-Y}$ concentration were obtained by performing short, high-temperature DMD simulation runs and saving configurations every 0.1×10^6 simulation steps. This protocol resulted in randomly placed and mixed peptides of each type that were used as initial populations for production runs (Fig. I in Supplementary Material). Multiple trajectories at each Aβ₁₋₄₂/Aβ$_{X-Y}$ concentration ratio were acquired at physiological temperature ($T = 0.13$) using the implicit solvent parameters $E_{HP} = 0.3$ and $E_{CH} = 0$ that best described the initial hydrophobic collapse into globular Aβ₁₋₄₂ oligomers. For each of the four Aβ$_{X-Y}$, five different molar concentration ratios were studied, resulting in 20 systems. For each system, eight trajectories of 20×10^6 simulation steps were acquired. The resulting Aβ₁₋₄₂ structures formed in the presence of Aβ$_{X-Y}$ molecules were quantified in terms of their secondary, tertiary, and quaternary structures and solvent exposure and compared to unaltered Aβ₁₋₄₂ oligomer structures derived previously.[25] Supplementary Methods in Supplementary Material provides a more detailed description of our computational approach and its limitations.

Supplementary Data

Supplementary data associated with this article can be found, in the online version, at doi:10.1016/j.jmb.2011.05.021

References

1. Hardy, J. & Selkoe, D. J. (2002). The amyloid hypothesis of Alzheimer's disease: progress and problems on the road to therapeutics. *Science*, **297**, 353–356.
2. Kirkitadze, M. D., Bitan, G. & Teplow, D. B. (2002). Paradigm shifts in Alzheimer's disease and other

neurodegenerative disorders: the emerging role of oligomeric assemblies. *J. Neurosci. Res.* **69**, 567–577.

3. Klein, W. L. (2002). ADDLs & protofibrils—the missing links? *Neurobiol. Aging*, **23**, 231–233.

4. Hardy, J. (2003). Alzheimer's disease: genetic evidence points to a single pathogenesis. *Ann. Neuro.* **54**, 143–144.

5. Klein, W. L., Stine, W. B. & Teplow, D. B. (2004). Small assemblies of unmodified amyloid β-protein are the proximate neurotoxin in Alzheimer's disease. *Neurobiol. Aging*, **25**, 569–580.

6. Glabe, C. G. (2005). Amyloid accumulation and pathogensis of Alzheimer's disease: significance of monomeric, oligomeric and fibrillar Aβ. *Subcell. Biochem.* **38**, 167–177.

7. Roychaudhuri, R., Yang, M., Hoshi, M. M. & Teplow, D. B. (2008). Amyloid β-protein assembly and Alzheimer disease. *J. Biol. Chem.* **284**, 4749–4753.

8. Rahimi, A., Shanmugam, A. & Bitan, G. (2008). Structure–function relationships of pre-fibrillar protein assemblies in Alzheimer's disease and related disorders. *Curr. Alzheimer Res.* **5**, 319–341.

9. Dahlgren, K. N., Manelli, A. M., Stine, W. B., Baker, L. K., Krafft, G. A. & LaDu, M. J. (2002). Oligomeric and fibrillar species of amyloid-β peptides differentially affect neuronal viability. *J. Biol. Chem.* **277**, 32046–32053.

10. Jarrett, J. T., Berger, E. P. & Lansbury, P. T. (1993). The carboxy terminus of the β amyloid protein is critical for the seeding of amyloid formation: implications for the pathogenesis of Alzheimer's disease. *Biochemistry*, **32**, 4693–4697.

11. Jarrett, J. T., Berger, E. P. & Lansbury, P. T. (1993). The C-terminus of the β protein is critical in amyloidogenesis. *Ann. N. Y. Acad. Sci.* **695**, 144–148.

12. Sawamura, N., Morishima-Kawashima, M., Waki, H., Kobayashi, K., Kuramochi, T., Frosch, M. P. *et al.* (2000). Mutant presenilin 2 transgenic mice. A large increase in the levels of Aβ 42 is presumably associated with the low density membrane domain that contains decreased levels of glycerophospholipids and sphingomyelin. *J. Biol. Chem.* **275**, 27901–27908.

13. Bitan, G., Kirkitadze, M. D., Lomakin, A., Vollers, S. S., Benedek, G. B. & Teplow, D. B. (2003). Amyloid β-protein (Aβ) assembly: Aβ40 and Aβ42 oligomerize through distinct pathways. *Proc. Natl Acad. Sci. USA*, **100**, 330–335.

14. Bernstein, S. L., Wyttenbach, T., Baumketner, A., Shea, J. E., Bitan, G., Teplow, D. B. *et al.* (2005). Amyloid β-protein: monomer structure and early aggregation states of Aβ42 and its Pro19 alloform. *J. Am. Chem. Soc.* **127**, 2075–2084.

15. Bernstein, S. L., Dupuis, N. F., Lazo, N. D., Wyttenbach, T., Condron, M. M., Bitan, G. *et al.* (2009). Amyloid-β protein oligomerization and the importance of tetramers and dodecamers in the aetiology of Alzheimer's disease. *Nat. Chem.* **1**, 326–331.

16. Gong, Y., Chang, L., Viola, K. L., Lacor, P. N., Lambert, M. P., Finch, C. E. *et al.* (2003). Alzheimer's disease-affected brain: presence of oligomeric Aβ ligands (ADDLs) suggests a molecular basis for reversible memory loss. *Proc. Natl Acad. Sci. USA*, **100**, 10417–10422.

17. Barghorn, S., Nimmrich, V., Striebinger, A., Krantz, C., Keller, P., Janson, B. *et al.* (2005). Globular amyloid

β-peptide₁₋₄₂ oligomer—a homogenous and stable neuropathological protein in Alzheimer's disease. *J. Neurochem.* **95**, 834–847.

18. Lesné, S., Koh, M. T., Kotilinek, L., Kayed, R., Glabe, C. G., Yang, A. *et al.* (2006). A specific amyloid-β protein assembly in the brain impairs memory. *Nature*, **440**, 352–357.

19. Ahmed, M., Davis, J., Aucoin, D., Sato, T., Ahuja, S., Aimoto, S. *et al.* (2010). Structural conversion of neurotoxic amyloid-β(1–42) oligomers to fibrils. *Nat. Struct. Mol. Biol.* **17**, 561–567.

20. Urbanc, B., Borreguero, J. M., Cruz, L. & Stanley, H. E. (2006). *Ab initio* discrete molecular dynamics approach to protein folding and aggregation. *Methods Enzymol.* **412**, 314–338.

21. Urbanc, B., Cruz, L., Ding, F., Sammond, D., Khare, S., Buldyrev, S. V. *et al.* (2004). Molecular dynamics simulation of amyloid β dimer formation. *Biophys. J.* **87**, 2310–2321.

22. Urbanc, B., Cruz, L., Yun, S., Buldyrev, S. V., Bitan, G., Teplow, D. B. *et al.* (2004). *In silico* study of amyloid β-protein folding and oligomerization. *Proc. Natl Acad. Sci. USA*, **101**, 17345–17350.

23. Yun, S., Urbanc, B., Cruz, L., Bitan, G., Teplow, D. B. & Stanley, H. E. (2007). Role of electrostatic interactions in amyloid β-protein (Aβ) oligomer formation: a discrete molecular dynamics study. *Biophys. J.* **92**, 4064–4077.

24. Lam, A., Teplow, D. B., Stanley, H. E. & Urbanc, B. (2008). Effects of the arctic (E22→G) mutation on amyloid β-protein folding: discrete molecular dynamics study. *J. Am. Chem. Soc.* **130**, 17413–17422.

25. Urbanc, B., Betnel, M., Cruz, L., Bitan, G. & Teplow, D. B. (2010). Elucidation of amyloid β-protein oligomerization mechanisms: discrete molecular dynamics study. *J. Am. Chem. Soc.* **132**, 4266–4280.

26. Lazo, N. D., Grant, M. A., Condron, M. C., Rigby, A. C. & Teplow, D. B. (2005). On the nucleation of amyloid β-protein monomer folding. *Protein Sci.* **14**, 1581–1596.

27. Murakami, K., Irie, K., Ohigashi, H., Hara, H., Nagao, M., Shimizu, T. *et al.* (2005). Formation and stabilization model of the 42-mer Aβ radical: implications for the long-lasting oxidative stress in Alzheimer's disease. *J. Am. Chem. Soc.* **127**, 15168–15174.

28. Krafft, G., Joyce, J., Jerecic, J., Lowe, R., Hepler, R., Nahas, D. D. *et al.* (2006). Design of Arrested-Assembly Aβ₁₋₄₂ Peptide Variants to Elucidate the ADDL Oligomerization Pathway and Conformational Specificity Of Anti-ADDL Antibodies 2006 Neuroscience Meeting Planner, Society for Neuroscience, Atlanta, GA; Program No. 509.5.

29. Yan, Y. & Wang, C. (2006). Aβ42 is more rigid than Aβ40 at the C terminus: implications for Aβ aggregation and toxicity. *J. Mol. Biol.* **364**, 853–862.

30. Sgourakis, N., Yan, Y., McCallum, S., Wang, C. & Garcia, A. (2007). The Alzheimer's peptides Aβ40 and 42 adopt distinct conformations in water: a combined MD/NMR study. *J. Mol. Biol.* **368**, 1448–1457.

31. Streltsov, V., Varghese, J., Masters, C. & Nuttall, S. (2011). Crystal structure of the amyloid-β p3 fragment provides a model for oligomer formation in Alzheimer's disease. *J. Neurosci.* **31**, 1419–1426.

32. Fradinger, E., Monien, B. H., Urbanc, B., Lomakin, A., Tan, M., Li, H. *et al.* (2008). C-terminal peptides

coassemble into Aβ42 oligomers and protect neurons against Aβ42-induced neurotoxicity. *Proc. Natl Acad. Sci. USA*, **105**, 14175–14180.

33. Li, H., Monien, B. H., Fradinger, E. A., Urbanc, B. & Bitan, G. (2010). Biophysicsl characterization of Aβ42 C-terminal fragments: inhibitors of Aβ42 neurotoxicity. *Biochemistry*, **49**, 1259–1267.

34. Wu, C., Murray, M. M., Bernstein, S. L., Condron, M. M., Bitan, G., Shea, J. *et al.* (2009). The structure of Aβ42 C-terminal fragments probed by a combined experimental and theoretical study. *J. Mol. Biol.* **387**, 492–501.

35. Li, H., Monien, B. H., Lomakin, A., Zemel1, R., Fradinger, E. A., Tan, M. *et al.* (2010). Mechanistic Investigation of the inhibition of Aβ42 assembly and neurotoxicity by c-terminal Aβ42 fragments. *Biochemistry*, **49**, 6358–6364.

36. McLaurin, J., Golomb, R., Jurewicz, A., Antel, J. P. & Fraser, P. E. (2000). Inositol stereoisomers stabilize an oligomeric aggregate of Alzheimer amyloid β peptide and inhibit Aβ-induced toxicity. *J. Biol. Chem.* **275**, 18495–18502.

37. McLaurin, J., Kierstead, M., Brown, M., Hawkes, C., Lambermon, M., Phinney, A. *et al.* (2006). Cyclohexanehexol inhibitors of Aβ aggregation prevent and reverse Alzheimer phenotype in a mouse model. *Nat. Med.* **12**, 801–808.

38. DaSilva, K., Shaw, J. & McLaurin, J. (2009). Amyloid-β fibrillogenesis: structural insight and therapeutic intervention. *Exp. Neurol.* **223**, 311–321.

39. Ladiwala, A., Lin, J., Bale, S., Marcelino-Cruz, A., Bhattacharya, M., Dordick, J. *et al.* (2010). Aromatic small molecules remodel toxic soluble oligomers of amyloid β through three independent pathways. *J. Biol. Chem.* **286**, 3209–3218.

40. Rezai-Zadeh, K., Shytle, D., Sun, N., Mori, T., Hou, H., Jeanniton, D. *et al.* (2005). Green tea epigallocatechin-3-gallate (EGCG) modulates amyloid precursor protein cleavage and reduces cerebral amyloidosis in Alzheimer transgenic mice. *J. Neurosci.* **25**, 8807–8814.

41. Ehrnhoefer, D. E., Bieschke, J., Boeddrich, A., Herbst, M., Masino, L., Lurz, R. *et al.* (2008). EGCG redirects amyloidogenic polypeptides into unstructured, off-pathway oligomers. *Nat. Struct. Mol. Biol.* **15**, 558–566.

42. Ladiwala, A., Lin, J., Bale, S., Marcelino-Cruz, A., Bhattacharya, M., Dordick, J. *et al.* (2010). Resveratrol selectively remodels soluble oligomers and fibrils of amyloid Aβ into off-pathway conformers. *J. Biol. Chem.* **285**, 24228–24237.

43. Teplow, D. B., Lazo, N. D., Bitan, G., Bernstein, S., Wyttenbach, T., Bowers, M. T. *et al.* (2006). Elucidating amyloid β-protein folding and assembly: a multidisciplinary approach. *Acc. Chem. Res.* **39**, 635–645.

44. Humphrey, W., Dalke, A. & Schulten, K. (1996). VMD: visual molecular dynamics. *J. Mol. Graphics*, **14**, 33–38.

45. Kirkitadze, M. D., Condron, M. M. & Teplow, D. B. (2001). Identification and characterization of key kinetic intermediates in amyloid β-protein fibrillogenesis. *J. Mol. Biol.* **312**, 1103–1119.

46. Ono, K., Condron, M. M. & Teplow, D. B. (2009). Structure–neurotoxicity relationships of amyloid β-protein oligomers. *Proc. Natl Acad. Sci. USA*, **106**, 14745–14750.

47. Chimon, S., Shaibat, M., Jones, C., Calero, D., Aizezi, B. & Ishii, Y. (2007). Evidence of fibril-like β-sheet structures in a neurotoxic amyloid intermediate of Alzheimer's β-amyloid. *Nat. Struct. Mol. Biol.* **14**, 1157–1164.

48. Wu, J. W., Breydo, L., Isas, J. M., Lee, J., Kuznetsov, Y. G., Langen, R. *et al.* (2010). Fibrillar oligomers nucleate the oligomerization of monomeric amyloid but do not seed fibril formation. *J. Biol. Chem.* **285**, 6071–6079.

49. Kawahara, M., Arispe, N., Kuroda, Y. & Rojas, E. (1997). Alzheimers-disease amyloid β-protein forms Zn²⁺-sensitive, cation-selective channels across excised membrane patches from hypothalamic neurons. *Biophys. J.* **73**, 67–75.

50. Demuro, A., Mina, E., Kayed, R., Milton, S. C., Parker, I. & Glabe, C. G. (2005). Calcium dysregulation and membrane disruption as a ubiquitous neurotoxic mechanism of soluble amyloid oligomers. *J. Biol. Chem.* **280**, 17294–17300.

51. D'Andrea, M. R. & Nagele, R. G. (2006). Targeting the alpha 7 nicotinic acetylcholine receptor to reduce amyloid accumulation in Alzheimer's disease pyramidal neurons. *Curr. Pharm. Des.* **12**, 677–684.

52. Shankar, G. M., Bloodgood, B. L., Townsend, M., Walsh, D. M., Selkoe, D. J. & Sabatini, B. L. (2007). Natural oligomers of the Alzheimer amyloid-β protein induce reversible synapse loss by modulating an NMDA-type glutamate receptor-dependent signaling pathway. *J. Neurosci.* **27**, 2866–2875.

53. Liu, R., Barkhordarian, H., Emadi, S., Park, C. P. & Sierks, M. (2005). Trehalose differentially inhibits aggregation and neurotoxicity of β-amyloid 40 and 42. *Neurobiol. Dis.* **20**, 74–81.

54. Luheshi, L. M., Tartaglia, G. G., Brorsson, A. C., Pawar, A. P., Watson, I. E., Chiti, F. *et al.* (2007). Systematic *in vivo* analysis of the intrinsic determinants of amyloid β pathogenicity. *PLoS Biol.* **5**, e290.

55. Jin, M., Shepardson, N., Yang, T., Chen, G., Walsh, D. & Selkoe, D. J. (2011). Soluble amyloid β-protein dimers isolated from Alzheimer cortex directly induce tau hyperphosphorylation and neuritic degeneration. *Proc. Natl Acad. Sci. USA*, **108**, 5819–5824.

56. Rapaport, D. C. (1997). *The Art of Molecular Dynamics Simulation*. Cambridge University Press, Cambridge, UK.

57. Smith, A. V. & Hall, C. K. (2001). α-Helix formation: discontinuous molecular dynamics on an intermediate-resolution protein model. *Proteins: Struct., Funct., Genet.* **44**, 344–360.

58. Ding, F., Borreguero, J. M., Buldyrev, S. V., Stanley, H. E. & Dokholyan, N. V. (2003). Mechanism for the α-helix to β-hairpin transition. *Proteins: Struct., Funct., Genet.* **53**, 220–228.

59. Berman, H. M., Westbrook, J., Feng, Z., Gilliland, G., Bhat, T. N., Weissig, H. *et al.* (2000). The Protein Data Bank. *Nucleic Acids Res.* **28**, 235–242. http://www.rcsb.org/pdb.